

Toward expanding the scope of radiology report summarization to multiple anatomies and modalities

Jean-Benoit Delbrouck

Maya Varma

Curtis P. Langlotz

Stanford University

JBDEL@STANFORD.EDU

MVARMA2@STANFORD.EDU

LANGLOTZ@STANFORD.EDU

Abstract

Radiology report summarization is a growing area of research. Given the Findings and/or Background sections of a radiology report, the goal is to generate a summary (called an Impression section) that highlights the key observations and conclusions of the radiology study. Recent efforts have released systems that achieve promising performance as measured by widely used summarization metrics such as BLEU and ROUGE. However, the research area of radiology report summarization currently faces important limitations. First, most of the results are reported on private datasets. This limitation prevents the ability to reproduce results and fairly compare different systems and solutions. Secondly, to the best of our knowledge, most research is carried out on chest X-rays. Sometimes, studies even omit to mention the concerned modality and anatomy in the radiology reports used for their experiments. To palliate these limitations, we propose a new dataset of six different modalities and anatomies based on the MIMIC-III database. We further release our results and the data splits used to carry out our experiments. Finally, we propose a simple report summarization system that outperforms the previous replicable research on the existing dataset.

Keywords: summarization; impressions; findings; radiology reports; language generation

there is prominence of the central pulmonary vasculature subtle prominence of the interstitial markings could relate to mild fluid overload [...]

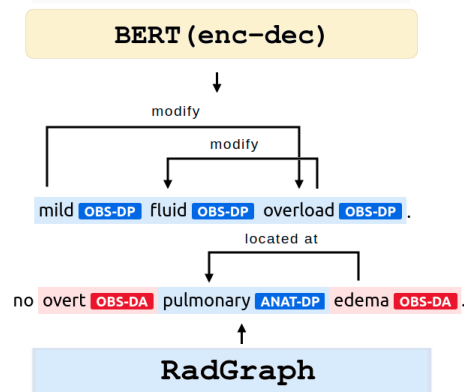


Figure 1: Illustration of our summarization pipeline. The model generates an impression from the findings and RadGraph creates semantic annotations used to evaluate the factual correctness of the impression.

1. Introduction

The radiology report documents and communicates crucial findings in a radiology study. A standard radiology report usually consists of a Background section that describes the exam and patient information, a Findings section, and an Impression section (Kahn Jr et al., 2009). In a typical workflow, a radiolo-

gist first dictates the detailed findings into the report and then summarizes the salient findings into the more concise Impression section based also on the condition of the patient. Automating this summarization task is critical because the Impression section is the most important part of a radiology report, and manual summarization can be time-consuming and error-prone.

Despite its importance, we identify three weaknesses in the ongoing work on radiology report summarization.

First, the most recent studies (Zhang et al., 2018, 2020; Hu et al., 2022) and organized challenges (Ben Abacha et al., 2021) on automated radiology report summarization systems solely focus on chest X-rays. The reason is that the only two open-access and curated datasets, namely MIMIC-CXR (Johnson et al., 2019) and Open-i Chest X-ray (Demner-Fushman et al., 2012), exclusively contain chest-X ray radiology reports. In some rarer cases, researchers omit to disclose the modality and anatomy of the radiology reports used for their experiments (Karn et al., 2022).

Secondly, existing models are optimized to generate summaries that achieve high performance on the ROUGE metric (Lin, 2004). As investigated in previous studies, this does not guarantee factually correct summaries (Zhang et al., 2020). So far, only one "factually-oriented" metric has been proposed, based on CheXbert (Smit et al., 2020). While this addition is a good step towards evaluating factual correctness of the summaries, it is limited to chest X-rays.

Finally, new proposed models (Karn et al., 2022; Hu et al., 2022) present an increased complexity in architecture that offers only marginal improvements on the existing evaluation metrics for summarization. This, in turn, makes the replication of studies more difficult.

To address these three limitations, we consequently present three contributions:

- We release a pre-processed and curated dataset of radiology reports for new modalities (MR and CT) and anatomies (Chest, Head, Neck, Sinus, Spine, Abdomen, Pelvis). Our dataset is based on the MIMIC-III database (Johnson et al., 2016) and suitable for radiology report summarization: each report contains a clear findings and impression section.
- We present a new summarization metric, called the RadGraph score, that evaluates the factual completeness and correctness of the generated radiology impressions. We show that this score is suitable for every modality and anatomy of our new dataset. We also show that the RadGraph score can be turned, without further modification, into a reward suitable for Reinforcement Learning (RL) optimization.
- We present a new simple summarization system that not only acts a strong baseline on the new datasets but also outperforms the previous replicable research on chest X-rays. Because our new system is small (few trainable parameters) and fast (low FLOPs), it makes it suitable for RL which is, by essence, computationally expensive.

Our paper is structured as follows: we first start by describing our three contribution, namely our new MIMIC-III summarization dataset (Section 2), the RadGraph score (Section 3) and our baseline model (Section 4). We then proceed to outline the experiments carried out (Section 5) and present our results (Section 6).

CT Abd-pelv	CT Chest	CT Head
15,989	12,786	31,402
CT Spine	MR Head	CT Neck
5,517	7,313	1,140
CT Sinus	Mr Spine	MR Abdomen
1,267	2,821	1,061
MR Neck	MR Pelvis	
230	253	

Table 1: Number of radiology reports (containing findings and impression pairs) for each new modality-anatomy, totaling 79,779 samples.

2. MIMIC-III summarization dataset

MIMIC-III (Johnson et al., 2016) is a large, freely-available database comprising de-identified health-related data associated with over forty thousand patients who stayed in critical care units of the Beth Israel Deaconess Medical Center between 2001 and 2012. This data comprises radiology reports from a wide range of modality (medical imaging techniques) and anatomy (body parts). To create a new radiology report summarization dataset, we first chose 5 of the most frequent modality/anatomy pairs in the pool of MIMIC-III reports, namely CT Head, CT Spine, CT Chest, CT Abdomen-Pelvis and MR head. We discard chest X-rays as they are included in the MIMIC-CXR dataset (Johnson et al., 2019). The number of samples per pair are available in Table 1 and constitute enough data to train a deep learning model. We also pick 6 less represented modality/anatomy pairs that could act as out-of-domain (OOD) test-sets, namely CT neck, CT sinus, MR Pelvis, MR Neck, MR Abdomen, MR Spine. This set of

pairs represents two levels of OOD: 1) the modality has not been seen during training (one could train on CT neck and test on MR Neck) 2) the anatomy has not been seen during training (for example, CT Sinus is the only “sinus” dataset).

For each report, we extract the findings and impression section. However, the findings section is not always stated as such. With the help of one board-certified radiologist, and for each modality/anatomy pair, we create a mapping of the section header that acts as “findings”. As an example, for CT head, findings could be referred as “non-contrast head ct”, “ct head”, “ct head without contrast”, “ct head without iv contrast”, “head ct”, “head ct without iv contrast” or “cta head”. This “findings” mapping contains up to 537 candidate sections for our whole dataset. We also discarded reports where multiple studies are pooled in the same radiology reports, leading to multiple intricate observations in the impression section. We release our mapping as well as the code to recreate the dataset from scratch (Appendix B).

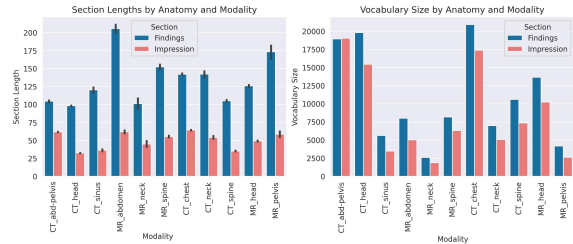


Figure 2: Section length and vocabulary size per anatomy-modality pairs.

In addition, a few comments can be made from Figure 2. As expected, for all anatomy-modality pairs, the findings section is significantly longer than the impression section (up to +315% for MR abdomen). The findings section of all our new pairs are also much

longer than chest X-rays: the MIMIC-CXR dataset averages 49 words per findings. In contrast, MR Abdomen and MR Pelvis average 205 and 174 words respectively. We can see note that CT Chest, CT Head and CT Abdomen-Pelvis have a relatively large vocabulary size (given their sample size) with respectively 20,909, 19,813 and 18,933. Surprisingly, the CT Abdomen-Pelvis impressions contains more vocabulary than the findings, as opposed to MR pelvis and MR abdomen impressions that contain respectively 36% and 37% less words than their findings counterpart.

3. RadGraph score

The goal of our RadGraph score is to provide an evaluation of the factual correctness and completeness of a generated impression. It does so by evaluating two semantic components of the impression: the correctness of the named entities and the relation between two entities.

We divide this section in two subsections: we first present RadGraph in section Section 3.1 and then describe how we leverage RadGraph to compute the proposed RadGraph score in section Section 3.2.

3.1. RadGraph

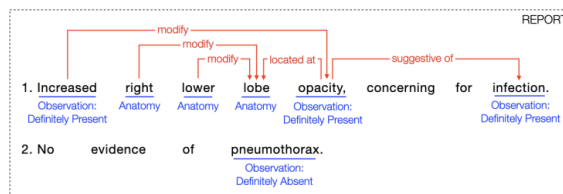


Figure 3: Example of the RadGraph annotations. Figure taken from Jain et al. (2021).

To design our new evaluation metric, we leverage the RadGraph dataset (Jain et al., 2021) containing board-certified radiologist annotations of chest X-ray reports, which correspond to 14,579 entities and 10,889 relations. RadGraph has released a PubMedBERT model (Gu et al., 2021) pretrained on these annotations to annotate new reports. An example of annotation can be seen in Figure 3. Before moving on to the next section, we quickly describe the concept of entities and relations:

Entities An entity is defined as a continuous span of text that can include one or more adjacent words. Entities in RadGraph center around two concepts: *Anatomy* and *Observation*. Three uncertainty levels exist for *Observation*, leading to four different entities: *Anatomy (ANAT-DP)*, *Observation: Definitely Present (OBS-DP)*, *Observation: Uncertain (OBS-U)*, and *Observation: Definitely Absent (OBS-DA)*.

Relations A relation is defined as a directed edge between two entities. Three levels exist: *Suggestive Of* (., .), *Located At* (., .), and *Modify* (., .).

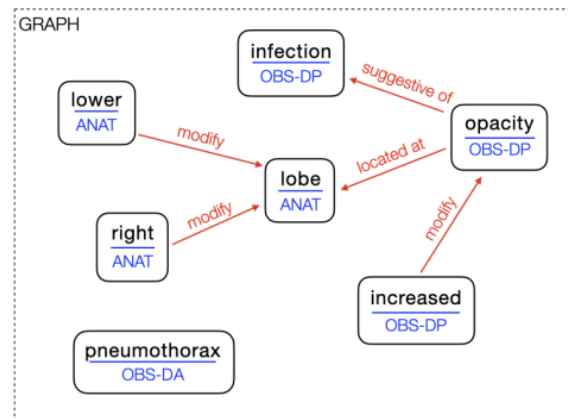


Figure 4: Graph view of the RadGraph annotations for the report in Figure 3.

MR Neck	CT Spine	MR Head
<p>slightly OBS-DP prominent OBS-DP lymph OBS-DP node OBS-DP in the posterior ANAT-DP chain ANAT-DP on the left side ANAT-DP side unchanged OBS-DP from previous examination . no definite evidence of infiltrating OBS-DA mass OBS-DA or definite pathologic adenopathy OBS-DA .</p>	<p>low resolution study reveals degenerative OBS-DP change OBS-DP and foraminal ANAT-DP narrowing OBS-DP without gross OBS-DA acute OBS-DA pathology OBS-DA</p>	<p>1 . no acute OBS-DA ischemia OBS-DA . 2 . age appropriate OBS-DP - appropriate atrophy OBS-DP , and chronic OBS-DP small OBS-DP vessel ANAT-DP ischemic OBS-DP changes OBS-DP . 3 . there is no occlusion OBS-DA or flow - limiting OBS-DA - limiting stenosis OBS-DA of the arterial ANAT-DP system ANAT-DP of the head and neck</p>

Table 2: Visualization of RadGraph’s model output (relations omitted) for a MR Neck (left), CT Spine (middle) and MR Neck (right) report.

3.2. Score

Using RadGraph annotation scheme and pretrained model, we design a F-score style reward that measures the factual consistency and completeness of the generated impression (also called hypothesis impression) compared to the reference impression.

To do so, we treat the RadGraph annotations of an impression as a graph $\mathcal{G}(V, E)$ with the set of nodes $V = \{v_1, v_2, \dots, v_{|V|}\}$ containing the entities and the set of edges $E = \{e_1, e_2, \dots, e_{|E|}\}$ the relations between pairs of entities. The graph is directed, meaning that the edge $e = (v_1, v_2) \neq (v_2, v_1)$. An example is depicted in Figure 4. Each node or edge of the graph also has a label, which we denote as v_{i_L} for an entity i (for example “OBS-DP” or “ANAT”) and e_{ij_L} for a relation $e = (v_i, v_j)$ (such as “modified” or “located at”).

To design our RadGraph score, we focus on the nodes V and whether or not a node has a relation in E . For a hypothesis impression y , we create a new set of triplets $T_y = \{(v_i, v_{i_L}, \mathcal{R})\}_{i=1:|V|}$. The value \mathcal{R} is 1 if $(v_i, v_j)_{j=1:|E|, i \neq j} \in E$, 0 otherwise. In other words, a triplet contains an entity, the entity label and whether or not this entity has a relation. We proceed to construct the same set for the reference report \hat{y} and denote this

set $T_{\hat{y}}$.

Finally, our score is defined as the harmonic mean of precision and recall between the hypothesis set T_y and the reference set $T_{\hat{y}}$, giving a value between 0 and 100. As an illustration, we provide in Appendix C the set V , E and T of the graph \mathcal{G} in Figure 4.

3.3. Generalization to other modalities and anatomies

As mentioned in Section 3.1, the RadGraph model is trained on chest X-rays entities and relations. Therefore, it is not obvious if RadGraph can be ported to other modalities and anatomies. As a partial validation of the use of RadGraph for our experiments, we ask one board-certified radiologist to subjectively evaluate the entities of the RadGraph model on two randomly selected reports for each anatomy-modality pairs. Three examples of those reports are shown in Table 2. In the selected reports, no entities were omitted by the RadGraph model.

4. Model

In this section, we detail our third contribution. We first describe in Section 4.1 our simple baseline by detailing the architecture of our findings-to-impression model and then explain in Section 4.2 how this model can

be trained using RL to directly optimize our RadGraph score.

4.1. Architecture

To encode the findings, we use a BERT encoder (Vaswani et al., 2017; Devlin et al., 2019) and use its final representation as textual features \mathbf{H} . To generate impressions, we use a BERT decoder with cross-attention over the textual features. More formally, the cross-attention of the decoder transformer layer is written:

$$\begin{aligned} \text{Cross-Attention}(Q, K, V) \\ = \text{softmax}\left(\frac{QK^\top}{\sqrt{d}}\right)V \end{aligned} \quad (1)$$

where Q is the decoder hidden state of size d and K and V are the textual features \mathbf{H} . We denote the number of layers in the BERT encoder and decoder as L .

The encoder can be pre-trained (i.e. using the pre-trained BioMed-RoBERTa (Gururangan et al., 2020) as encoder and decoder, for example) in which case the number of layers L is defined by the pre-trained model. We can also train both the encoder and decoder from scratch with a custom number of layers L . More details are available in our Experiment section.

4.2. Training

If we denote θ as the model parameters, then θ is learned by maximizing the likelihood of the hypothesis impression $\mathbf{Y} = (\mathbf{y}_1, \mathbf{y}_2, \dots, \mathbf{y}_n)$ or in other words by minimizing the negative log likelihood (NLL). The objective function is given by:

$$\mathcal{L}(\theta) = - \sum_{t=1}^n \log p_{\theta}(\mathbf{y}_t | \mathbf{y} < t, \mathbf{H}) \quad (2)$$

After the NLL training, we start a RL training by optimizing our RadGraph score. The loss function in Equation (2) is now given by:

$$\mathcal{L}(\theta) = -\mathbb{E}_{\mathbf{Y} \sim p_{\theta}} \mathbf{r}(\mathbf{Y}) \quad (3)$$

where $\mathbf{r}(\mathbf{Y})$ is the reward given of the generated report. We use the SCST algorithm (Rennie et al., 2017) to approximate the expected gradient of our non-differentiable reward function. The expression becomes:

$$\nabla_{\theta} \mathcal{L}(\theta) \approx -(\mathbf{r}(\mathbf{Y}) - \mathbf{r}(\bar{\mathbf{Y}})) \nabla_{\theta} \log_{p_{\theta}}(\mathbf{Y}) \quad (4)$$

Here $\mathbf{r}(\bar{\mathbf{Y}})$ acts a baseline (Sutton et al., 1998) to reduce the variance of $\mathbf{r}(\mathbf{Y})$. In our case, $\mathbf{r}(\bar{\mathbf{Y}})$ is the expected reward by sampling from the model during training.

5. Experiments

In this section, we detail the experiments carried out to evaluate our three contributions.

5.1. Model

For our BERT encoder-decoder of Section 4.1, we use two pre-trained model: BioMed-RoBERTa (Gururangan et al., 2020) and PubMedBERT (Gu et al., 2021), and also train from scratch using $L = 2$, $L = 4$ and $L = 8$. When training from scratch, the rest of the model parameters can be found in Appendix D.

The details of NLL and RL training can be found in Appendix E.

5.2. Datasets

MIMIC-CXR To compare our baselines with the state-of-the-art, we run summarization experiments on the MIMIC-CXR dataset (Johnson et al., 2019), using the official splits. MIMIC-CXR contains 128,003 reports with findings and impression split as follows: 125,388 for train, 991 for validation and 1,624 for testing.

MIMIC-III For training, we use the CT abdomen/pelvis, CT Chest, CT Neck, CT Spine, CT Head and MR Head splits as they contain enough training data to train our models. The last splits, namely MR Pelvis, MR Spine, MR Neck, MR Abdomen and CT Sinus are used as test-sets.

5.3. Metrics

We proceed to evaluate our systems using the ROUGE1, ROUGE2 and ROUGEL metrics (Lin, 2004) to be consistent with prior work. We also report the RadGraph score (Section 3) for both the MIMIC-CXR and MIMIC-III experiments.

For MIMIC-CXR, we also use F_1 CheXbert (Zhang et al., 2020) score alongside our RadGraph score to evaluate

the factual correctness of the generated impressions. This metric uses CheXbert (Smit et al., 2020), a Transformer-based model trained to output abnormalities of chest X-rays given a radiology report (or an impression) as input. F_1 CheXbert is the f1-score between the prediction of CheXbert over the hypothesis impression \hat{y} and the corresponding reference impression y . The f1-score is calculated over the 14 abnormalities to be consistent with Hu et al. (2022). Because the abnormalities are specific to chest X-rays, we only use it for MIMIC-CXR.

6. Results

This section is divided in two parts. First, we show the results of our preliminary experiments on MIMIC-CXR to validate our

Model	Test Scores				
	ROUGE1	ROUGE2	ROUGEL	F_1 CheXbert	RadGraph
MIMIC-CXR					
Liu and Lapata (2019)	47.16	32.31	45.47	—	—
Hu et al. (2021)	48.37	33.34	46.68	69.15	44.20
Hu et al. (2022)	51.02	35.21	46.65	70.73	45.23
BioMedRoBERTa (NLL)	45.86	29.80	42.10	65.90	38.31
PubMedBERT (NLL)	48.30	33.18	46.25	68.20	44.80
L2 (NLL)	48.84	34.20	44.86	70.01	44.09
L4 (NLL)	50.12	35.12	46.82	71.25	45.95
L8 (NLL)	51.14	34.38	46.25	69.12	44.94
L4 (RL)	51.96	35.65	47.10	74.86	48.23
MIMIC-III					
L4 (NLL, MR Head)	35.84	16.20	27.50	—	22.50
L4 (NLL, CT Abd/Pel)	27.62	7.85	19.69	—	13.02
L4 (NLL, CT Chest)	33.62	13.13	25.01	—	22.19
L4 (NLL, CT Neck)	24.36	8.95	20.78	—	10.06
L4 (NLL, CT Head)	41.09	23.25	35.29	—	32.62

Table 3: Summary of our results discussed throughout Section 6. Each reported score is the average of 5 independent runs. NLL refers to Equation (2), RL refers to Equation (4).

baselines and training setup (Figure 6.1. We then discuss the results on our new MIMIC-III dataset.

6.1. Preliminary experiments on MIMIC-CXR

The results of our preliminary experiments on MIMIC-CXR can be found in Table 3.

(NLL) When training with NLL, our best performing model is $L = 4$, meaning our BERT encoder-decoder trained from scratch with four hidden layers. For the factual-correctness metrics, this model achieves 71.25 points of F_1 CheXbert and 45.95 points of RadGraph score. This difference is respectively of +0.52 and +1.15 points compared to Hu et al. (2022) and +1.13 and +1.01 compared to our biggest model $L = 8$. The model $L = 4$ also reports the highest ROUGE-L: 46.82. These metrics can be further improved when ensembling models:

Surprisingly, using BioMedRoBERTa and PubMedBERT as pre-training didn’t help improve our results. On the contrary, they report the lowest score of all our model variants. Nevertheless, this aligns with the low results from Liu and Lapata (2019) where authors also used pre-trained BERT encoder and decoder for their summarization. In addition, in the task of Radiology Report Generation (X-ray to impression), Miura et al. (2021) reported the strongest performances using a one-layered BERT decoder.

(RL) Using RL to directly optimize the RadGraph score further improved the metrics accross the board. Compared to L4 (NLL), L4 (RL) reports an improvement of +2.28 (+4.96%) RadGraph score, +3.61 (+5.1%) F_1 CheXbert but only +0.28 (+0.5%) ROUGE-L. Figure 5 shows that our L4 (RL) model is also encouraged to generate more en-

tities and relations than its NLL counterpart. However, L4 (RL) generated more "ANAT-DP" entities and "located at" relations than found in the reference. Conversely, it didn’t generate any "OSB-U" and "suggestive-of". One hypothesis is that, because "OSB-U" and "suggestive-of" are under-represented in the dataset, the RL model couldn’t learn to use it correctly, leading to a negative reward, making in turn the model less and less likely to use it.

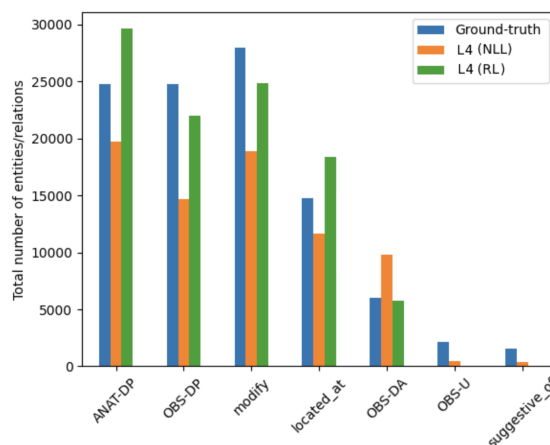


Figure 5: Number of entities and relations generated by our models L4 (NLL) and L4 (RL) on the MIMIC-CXR test set, compared to the reference (blue)

Given these encouraging results, we decide to carry out the remaining of our experiments using the L4 model.

6.2. Experiments on MIMIC-III

The results of our experiments on MIMIC-III can be found in Table 3 (NLL) and Table 5 (RL).

(NLL) Overall, the scores are lower than the MIMIC-CXR experiments. Two reasons explain this trend: 1) all MIMIC-III datasets contain fewer training samples, and 2)

L4 (NLL):	no significant change in degree of intraventricular hemorrhage compared to prior study
L4 (RL):	1 no evidence of acute intraventricular hemorrhage or mass effect 2 no evidence of acute bleed
Reference:	stable appearance of large intraventricular hemorrhage with no evidence of obstructive hydrocephalus or new bleed.

Table 4: Cherry picked generated CT HEAD impressions from our models and its reference.

as shown in Figure 2, the findings and impressions in the MIMIC-III datasets are substantially longer than MIMIC-CXR. Hence, the summarization task is more difficult. As an example, we highlight in Table 4 generated impression of by two of our models. Such examples show that our model L4 (NLL) has learned, to some extent, to summarize effectively. A more in-depth study would be required to evaluate the output on the whole test-set, for different modalities and anatomies.

(RL) As shown in Table 5, directly optimizing the RadGraph score using Reinforcement Learning improves the ROUGE and RadGraph score for all modalities and anatomies. It shows convincingly that RadGraph can be used, either as a score to evaluate the radiology reports or as reward to optimize factual correctness, for various types of reports.

7. Conclusion

In this paper, we present three original contributions to address the current weakness of the task of Radiology Report Summarization. First, we release a pre-processed and curated dataset of radiology reports for new modalities (MR and CT) and anatomies (Chest,

	ROUGE	RadGraph score
MR Head	29.10 (+5.8%)	24.19 (+7.5%)
CT ab/p	21.32 (+8.2%)	15.10 (+14.3%)
CT Chest	25.50 (+1.5%)	25.06 (+12.9%)
CT Neck	21.18 (+1.9%)	12.56 (+24.8%)
CT Head	35.52 (+0.6%)	34.95 (+6.1%)

Table 5: Performance of our L4 (RL) on the five largest sets of our MIMIC-III summarization dataset with improvements in % compared to their NLL counterpart from Table 3

Head, Neck, Sinus, Spine, Abdomen, Pelvis) based MIMIC-III database (Section 2). This allows future research to extend the scope of this task beyond chest x-rays. Then, we presented a new summarization metric, called the RadGraph score (Section 3), that evaluates the factual completeness and correctness of the generated radiology impressions. We showed theoretically (Section 3.3) and empirically (Section 6.2) that this new evaluation metric was suitable for every modality and anatomy of our new dataset.

Finally, we presented a new simple summarization system (Section 4.1) that not only acted a strong baseline on the new datasets but also outperforms the previous replicable research on chest X-rays (Section 6). Our model, the dataset, and the score can be found and replicated in Appendix B.

8. Future work

RadGraph has shown to be an efficient tool and could be used in different ways than presented in this paper. One could train a general model on the most frequent modalities to test its performance on the ood test-sets, namely CT neck, CT sinus, MR Pelvis, MR Neck, MR Abdomen, MR Spine. The goal is to evaluate if knowledge can be transferred to unseen modalities and anatomies.

References

- Asma Ben Abacha, Yassine Mrabet, Yuhao Zhang, Chaitanya Shivade, Curtis Langlotz, and Dina Demner-Fushman. Overview of the MEDIQA 2021 shared task on summarization in the medical domain. In *Proceedings of the 20th Workshop on Biomedical Language Processing*, pages 74–85, Online, June 2021. Association for Computational Linguistics. doi: 10.18653/v1/2021.bionlp-1.8. URL <https://aclanthology.org/2021.bionlp-1.8>.
- Jean-benoit Delbrouck, Khaled Saab, Maya Varma, Sabri Eyuboglu, Pierre Chambon, Jared Dunnmon, Juan Zambrano, Akshay Chaudhari, and Curtis Langlotz. ViLMedic: a framework for research at the intersection of vision and language in medical AI. In *Proceedings of the 60th Annual Meeting of the Association for Computational Linguistics: System Demonstrations*, pages 23–34, Dublin, Ireland, May 2022. Association for Computational Linguistics. doi: 10.18653/v1/2022.acl-demo.3. URL <https://aclanthology.org/2022.acl-demo.3>.
- Dina Demner-Fushman, Sameer Antani, Matthew Simpson, and George R Thoma. Design and development of a multimodal biomedical information retrieval system. *Journal of Computing Science and Engineering*, 6(2):168–177, 2012.
- Jacob Devlin, Ming-Wei Chang, Kenton Lee, and Kristina Toutanova. BERT: Pre-training of deep bidirectional transformers for language understanding. In *Proceedings of the 2019 Conference of the North American Chapter of the Association for Computational Linguistics: Human Language Technologies, Volume 1 (Long and Short Papers)*, pages 4171–4186, Minneapolis, Minnesota, June 2019. Association for Computational Linguistics. doi: 10.18653/v1/N19-1423. URL <https://aclanthology.org/N19-1423>.
- Yu Gu, Robert Tinn, Hao Cheng, Michael Lucas, Naoto Usuyama, Xiaodong Liu, Tristan Naumann, Jianfeng Gao, and Hoifung Poon. Domain-specific language model pre-training for biomedical natural language processing. *ACM Transactions on Computing for Healthcare (HEALTH)*, 3(1):1–23, 2021.
- Suchin Gururangan, Ana Marasović, Swabha Swayamdipta, Kyle Lo, Iz Beltagy, Doug Downey, and Noah A. Smith. Don’t stop pretraining: Adapt language models to domains and tasks. In *Proceedings of ACL*, 2020.
- Jinpeng Hu, Jianling Li, Zhihong Chen, Yaling Shen, Yan Song, Xiang Wan, and Tsung-Hui Chang. Word graph guided summarization for radiology findings. In *Findings of the Association for Computational Linguistics: ACL-IJCNLP 2021*, pages 4980–4990, Online, August 2021. Association for Computational Linguistics. doi: 10.18653/v1/2021.findings-acl.441. URL <https://aclanthology.org/2021.findings-acl.441>.
- Jinpeng Hu, Zhuo Li, Zhihong Chen, Zhen Li, Xiang Wan, and Tsung-Hui Chang. Graph enhanced contrastive learning for radiology findings summarization. In *Proceedings of the 60th Annual Meeting of the Association for Computational Linguistics (Volume 1: Long Papers)*, pages 4677–4688, 2022.
- Saahil Jain, Ashwin Agrawal, Adriel Saporta, Steven Truong, Du Nguyen Duong, Tan Bui, Pierre Chambon, Yuhao Zhang, Matthew Lungren, Andrew Ng, Curtis Langlotz, Pranav Rajpurkar, and Pranav Rajpurkar. Radgraph: Extracting clinical entities and relations from radiology reports. In J. Vanschoren and S. Yeung, edi-

- tors, *Proceedings of the Neural Information Processing Systems Track on Datasets and Benchmarks*, volume 1, 2021.
- Alistair E. W. Johnson, Tom J. Pollard, Nathaniel R. Greenbaum, Matthew P. Lungren, Chih-ying Deng, Yifan Peng, Zhiyong Lu, Roger G. Mark, Seth J. Berkowitz, and Steven Horng. MIMIC-CXR-JPG, a large publicly available database of labeled chest radiographs. *arXiv e-prints*, art. arXiv:1901.07042, January 2019.
- Alistair EW Johnson, Tom J Pollard, Lu Shen, Li-wei H Lehman, Mengling Feng, Mohammad Ghassemi, Benjamin Moody, Peter Szolovits, Leo Anthony Celi, and Roger G Mark. Mimic-iii, a freely accessible critical care database. *Scientific data*, 3(1):1–9, 2016.
- Alistair EW Johnson, Tom J Pollard, Seth J Berkowitz, Nathaniel R Greenbaum, Matthew P Lungren, Chih-ying Deng, Roger G Mark, and Steven Horng. Mimic-cxr, a de-identified publicly available database of chest radiographs with free-text reports. *Scientific data*, 6(1):1–8, 2019.
- Charles E Kahn Jr, Curtis P Langlotz, Elizabeth S Burnside, John A Carrino, David S Channin, David M Hovsepian, and Daniel L Rubin. Toward best practices in radiology reporting. *Radiology*, 252(3):852–856, 2009.
- Sanjeev Kumar Karn, Ning Liu, Hinrich Schütze, and Oladimeji Farri. Differentiable multi-agent actor-critic for multi-step radiology report summarization. In *Proceedings of the 60th Annual Meeting of the Association for Computational Linguistics (Volume 1: Long Papers)*, pages 1542–1553, 2022.
- Chin-Yew Lin. Rouge: A package for automatic evaluation of summaries. In *Text summarization branches out*, pages 74–81, 2004.
- Yang Liu and Mirella Lapata. Text summarization with pretrained encoders. In *Proceedings of the 2019 Conference on Empirical Methods in Natural Language Processing and the 9th International Joint Conference on Natural Language Processing (EMNLP-IJCNLP)*, pages 3730–3740, Hong Kong, China, November 2019. Association for Computational Linguistics. doi: 10.18653/v1/D19-1387. URL <https://aclanthology.org/D19-1387>.
- Yasuhide Miura, Yuhao Zhang, Emily Tsai, Curtis Langlotz, and Dan Jurafsky. Improving factual completeness and consistency of image-to-text radiology report generation. In *Proceedings of the 2021 Conference of the North American Chapter of the Association for Computational Linguistics: Human Language Technologies*, pages 5288–5304, 2021.
- Steven J Rennie, Etienne Marcheret, Youssef Mroueh, Jerret Ross, and Vaibhava Goel. Self-critical sequence training for image captioning. In *Proceedings of the IEEE conference on computer vision and pattern recognition*, pages 7008–7024, 2017.
- Akshay Smit, Saahil Jain, Pranav Rajpurkar, Anuj Pareek, Andrew Y Ng, and Matthew Lungren. Combining automatic labelers and expert annotations for accurate radiology report labeling using bert. In *Proceedings of the 2020 Conference on Empirical Methods in Natural Language Processing (EMNLP)*, pages 1500–1519, 2020.
- Richard S Sutton, Andrew G Barto, et al. Introduction to reinforcement learning. *MIT press Cambridge*, 1998.
- Ashish Vaswani, Noam Shazeer, Niki Parmar, Jakob Uszkoreit, Llion Jones, Aidan N

Gomez, Łukasz Kaiser, and Illia Polosukhin. Attention is all you need. *Advances in neural information processing systems*, 30, 2017.

Thomas Wolf, Lysandre Debut, Victor Sanh, Julien Chaumond, Clement Delangue, Anthony Moi, Pierric Cistac, Tim Rault, Rémi Louf, Morgan Funtowicz, et al. Transformers: State-of-the-art natural language processing. In *Proceedings of the 2020 conference on empirical methods in natural language processing: system demonstrations*, pages 38–45, 2020.

Yuhao Zhang, Daisy Yi Ding, Tianpei Qian, Christopher D Manning, and Curtis P Langlotz. Learning to summarize radiology findings. In *Proceedings of the Ninth International Workshop on Health Text Mining and Information Analysis*, pages 204–213, 2018.

Yuhao Zhang, Derek Merck, Emily Tsai, Christopher D Manning, and Curtis Langlotz. Optimizing the factual correctness of a summary: A study of summarizing radiology reports. In *Proceedings of the 58th Annual Meeting of the Association for Computational Linguistics*, pages 5108–5120, 2020.

Yuhao Zhang, Yuhui Zhang, Peng Qi, Christopher D Manning, and Curtis P Langlotz. Biomedical and clinical english model packages for the stanza python nlp library. *Journal of the American Medical Informatics Association*, 28(9):1892–1899, 2021.

Appendix A. Related work

We restrict this section to Radiology Report Summarization.

The first attempt at automatic summarization of radiology finding into natural language impression statements is proposed by Zhang et al. (2018). Their contribution is to propose a first baseline on the task, using a bidirectional-LSTM as encoder and decoder. Importantly, they found that about 30% of the radiology summaries generated from neural models contain factual errors. Subsequently, Zhang et al. (2020) proposed the F₁CheXbert score to evaluate the factual correctness of the generated impression. They also use RL to directly optimize that metric. Finally, both Hu et al. (2021) and Hu et al. (2022) used the Biomedical and Clinical English Model Packages in the Stanza Python NLP Library (Zhang et al., 2021) to extract medical entites. The former study used the entities to construct a Graph Neural Network, used as input in their summarization pipeline, while the latter study used the entites to mask the findings in a contrastive pre-training.

We believe this paper is an original contribution to the aforementioned work. As instigated by Zhang et al. (2018), our goal is to release new summarization corpus and baselines on new modalities and anatomies. We do so by releasing 11 new anatomy-modality pairs. Similarly to Zhang et al. (2020), we continue the effort in proposing a new metric that evaluate the factual correctness and completeness of the generated impression, namely the RadGraph score. Finally, we improve the work of Hu et al. (2021) and Hu et al. (2022) in two ways: 1) we use semantic annotations from a pre-trained model supervised on board-certified radiologists annotations, as opposed to Stanza that leverages unsupervised biomedical and clinical text data 2) we

leverage relation annotations between entities, a feature that was not available to prior work.

Appendix B. Code and data release

To help with further research, we also make our code publicly available. More specifically, we release the code of the RadGraph score as well as the training of our baseline. We also release the script to download, pre-process and split the radiology reports of the MIMIC-III database as per our experiments.

To download the MIMIC-III database, researchers are required to formally request access via a process documented on the MIMIC website. There are two key steps that must be completed before access is granted:

- 1) the researcher must complete a recognized course in protecting human research participants that includes Health Insurance Portability and Accountability Act (HIPAA) requirements.
- 2) the researcher must sign a data use agreement, which outlines appropriate data usage and security standards, and forbids efforts to identify individual patients.

Our research has been carried out using the ViLMedic library (Delbrouck et al., 2022). Our code is available at <https://github.com/jbdel/vilmedic>. This link is anonymized and complies with the double blind review process.

Appendix C. Set \bar{V} of Figure 4

$V = \{\text{mild, fluid, overload, overt, pulmonary, edema}\}$
 $E = \{(\text{mild, overload}), (\text{overload, fluid}), (\text{edema, pulmonary})\}$

$T = \{(\text{mild}, \text{obs-dp}, 1), (\text{fluid}, \text{obs-dp}, 0),$
 $(\text{overload}, \text{obs-dp}, 1), (\text{overt}, \text{obs-da}, 0),$
 $(\text{pulmonary}, \text{anat-dp}, 0), (\text{edema}, \text{obs-da}, 1)\}$

Appendix D. Model hyper-parameters

Our model is built using HuggingFace (Wolf et al., 2020). For reference, the following configuration declares 40.77M training parameters for $L = 2$.

```

{
  encoder:
    attention_probs_dropout_prob: 0.1
    hidden_act: gelu
    hidden_dropout_prob: 0.1
    hidden_size: 768
    initializer_range: 0.02
    intermediate_size: 3072
    layer_norm_eps: 1e-05
    max_position_embeddings: 514
    num_attention_heads: 12
    num_hidden_layers: L
    position_embedding_type: absolute
  decoder:
    add_cross_attention: true
    attention_probs_dropout_prob: 0.1
    hidden_act: gelu
    hidden_dropout_prob: 0.1
    hidden_size: 768
    initializer_range: 0.02
    intermediate_size: 3072
    layer_norm_eps: 1e-05
    max_position_embeddings: 514
    num_attention_heads: 12
    num_hidden_layers: L
    position_embedding_type: absolute
}
    
```

Listing 1: Model parameters

Appendix E. Training hyper-parameters

For NLL and RL training, we use the following hyper-parameters (number of bert layers $L = 4$):

```

{
  batch_size (mimic-cxr): 128
  batch_size (mimic-iii): 24
  optimizer: Adam
  optim_params:
    lr: 1e-4
    weight_decay: 0.
  lr_decay: ReduceLROnPlateau
  lr_decay_params:
    factor: 0.8
    patience: 1
    min_lr: 0.000001
  threshold_mode: abs
}
    
```

Listing 2: Training parameters

The ReduceLROnPlateau scheduler is on the ROUGE metric for NLL training and RadGraph score for RL training.

During RL training, the reward $r(\mathbf{Y})$ at Equation (3) is computed as $0.01 * \text{NLL loss} + 0.495 * \text{BERTSCORE} + 0.495 * \text{RadGraph score}$ as suggested by Miura et al. (2021). If one optimizes a factual metric based on entities alone, then the model is not encouraged to keep a correct grammatical structure.